


## Visualizing the localized electrons of a kagome flat band

Caiyun Chen,<sup>\*</sup> Jiangchang Zheng,<sup>\*</sup> Ruopeng Yu,<sup>✉,\*</sup> Soumya Sankar,<sup>✉</sup> Kam Tuen Law, Hoi Chun Po, and Berthold Jäck<sup>✉†</sup>  
*Department of Physics, The Hong Kong University of Science and Technology, Clear Water Bay, Kowloon, Hong Kong SAR*

 (Received 30 July 2023; revised 16 November 2023; accepted 26 November 2023; published 20 December 2023)

Destructive interference between electron wavefunctions on the two-dimensional kagome lattice induces an electronic flat band, which could host a variety of interesting quantum states. Key to realize these proposals is to demonstrate the real-space localization of kagome flat-band electrons. The extent to which the complex structure of realistic materials counteract the localizing effect of destructive interference is hitherto unknown. Moreover, a detailed understanding of the real-space distribution of the electronic states of kagome flat bands has not been developed yet. We used scanning tunneling microscopy to visualize the kagome flat band at the surface of CoSn, a kagome metal. Consistent with results from model calculations, we find that the local density of states associated with the kagome flat bands exhibits a unique real-space distribution by which it can be distinguished from the local density of states of dispersive electron bands and trivially localized states, such as well-localized orbitals and surface resonances. Our results further show that these states exhibit an extremely small localization length of two to three angstroms concomitant with a strongly renormalized quasiparticle velocity  $v \approx 1 \times 10^4$  m/s, comparable to that of moiré superlattices. Our findings provide fundamental insight into the electronic properties of kagome metals and present a key step for future research on emergent many-body states in these systems.

DOI: [10.1103/PhysRevResearch.5.043269](https://doi.org/10.1103/PhysRevResearch.5.043269)

### I. INTRODUCTION

Electrons occupying flat bands in momentum space are expected to be localized in real space. Hence, materials with electronic flat bands present an attractive venue to explore many-body quantum states that can arise from Coulomb interactions. To date, much interest has been directed to the study of these states in moiré flat bands [1–4]. The two-dimensional kagome lattice model, realized through a set of corner sharing triangles [see Fig. 1(a)], offers an alternative way to realize a topological flat band [6,7]. Here, destructive interference between electron wavefunctions is predicted to result in electronic states with nontrivial real-space Wannier functions [8], which are localized at atomic length scales. Despite earlier attempts to image these states in various materials with a kagome lattice structure [9–12], experimental evidence of these characteristics is still missing and a detailed theoretical understanding of the real-space distribution of the flat-band eigenstates has not been yet developed. These insights will be key toward the realization of various interesting quantum phases, such as zero-field fractional quantum Hall states [13,14].

The kagome metals of the FeSn family have attracted significant interest, because the judicious choice of constituent elements and stoichiometry permits control of the electronic,

magnetic, and topological properties [8,15–19]. CoSn was identified as a particularly promising candidate [20] in which an advantageous layer stacking sequence permits a set of weakly dispersing bands near Fermi energy ( $E_F$ ) that were associated with a kagome flat band [8,17,21]. Recent theoretical work suggests that the coupling between the Co  $d$ -orbitals and Sn  $p$ -orbitals indeed favors the presence of two  $d$ -orbital derived flat bands near Fermi energy [22]. However, it is important to appreciate that realistic materials deviate from the 2D kagome lattice model; the electronic coupling in the out-of-plane direction, a more complex lattice structure, and spin-orbit coupling could weaken the electron localization. The inherent interest in flat-band systems is in the potential amplification of interaction effects between localized charge carriers. The effective interaction strength is strongly affected by the degree of localization of the relevant orbitals, and how it suffers from these deteriorating effects is not known so far.

Here, we perform the real-space characterization of the Wannier states of a native kagome flat band using STM. Such measurements are particularly suited to study the energy-resolved local electronic density of states (LDOS) at atomic resolution and previously helped characterize the flat bands of moiré superlattices [23,24]. In this paper, we use spectroscopic imaging with the STM on the surface of CoSn thin films to visualize the real-space localization of kagome flat-band electronic states. Interestingly, our study finds that the destructive interference-based localization mechanism in a kagome lattice results in a unique real-space LDOS distribution of  $d$ -orbital-derived flat bands. Going beyond a bandwidth characterization in momentum space [8,17], the high spatial resolution of STM enables us to directly visualize and quantitatively investigate this distinct LDOS distribution, by which it can be distinguished from those of dispersive electronic bands, well-localized orbitals, and surface resonances.

<sup>\*</sup>These authors contributed equally to this work.

<sup>†</sup>bjaeck@ust.hk

*Published by the American Physical Society under the terms of the Creative Commons Attribution 4.0 International license. Further distribution of this work must maintain attribution to the author(s) and the published article's title, journal citation, and DOI.*

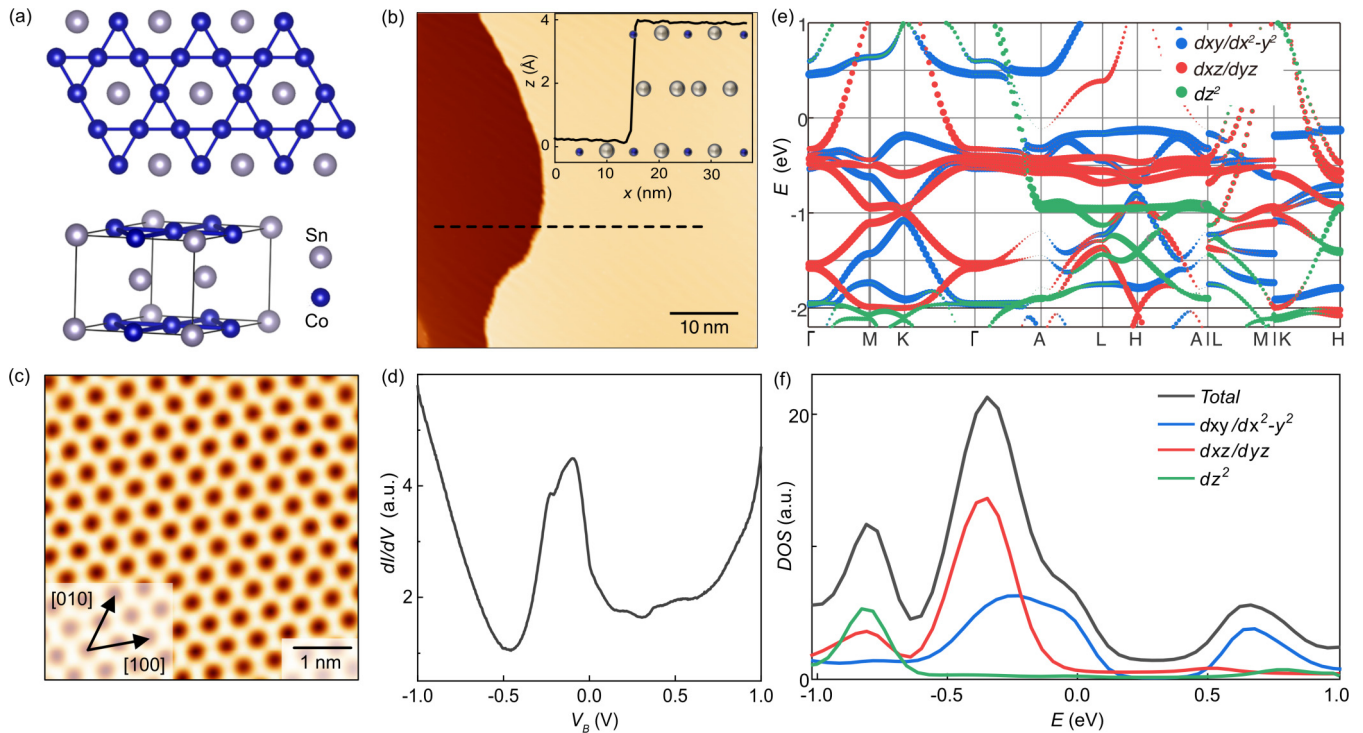


FIG. 1. (a) CoSn lattice structure. (Upper panel)  $\text{Co}_3\text{Sn}$  kagome layer within the crystallographic  $a$ - $b$  plane (silver sphere: Sn; blue sphere: Co). (Lower panel)  $\text{Co}_3\text{Sn}$  and stanene  $\text{Sn}_2$  layers are stacked in alternating order along the crystallographic  $c$  axis. (b) STM topography of the as-grown CoSn thin film surface ( $I = 50$  pA,  $V_B = -1.5$  V). (Inset) Topographic height  $z$  recorded along the black dashed line. (c) Magnified STM topography of the  $\text{Co}_3\text{Sn}$  surface ( $I = 3$  nA,  $V_B = 0.3$  V). (d) Typical  $dI/dV$  spectrum recorded on top of the  $\text{Co}_3\text{Sn}$  surface ( $I = 3$  nA, lock-in modulation  $V_m = 10$  mV). (e) Energy  $E$  resolved spectral function of CoSn obtained from density functional theory calculations along the crystallographic high-symmetry directions (see the Supplemental Material [5]). The orbital character of the bands is color-encoded (see legend). The calculation includes 2% tensile strain along the crystallographic [010] direction. (f) The calculated total and orbital-resolved density of states (DOS) of the Co  $d$  orbital derived bands shown in panel (e).

## II. RESULTS

CoSn ( $P6/mmm$  space group,  $a = 5.25$  Å,  $c = 4.19$  Å) crystallizes in a hexagonal lattice structure that consists of alternating  $\text{Sn}_2$  honeycomb (stanene) and  $\text{Co}_3\text{Sn}$  kagome layers. We prepared CoSn thin films (nominal thickness  $d = 50$  nm) on the surface of niobium (Nb) doped  $\text{SrTiO}_3$  (111) by using molecular beam epitaxy (MBE) (see the Supplemental Material, SM [5]). The Vollmer-Weber growth mode results in flat top islands with typical diameters of few hundreds of nanometers. STM measurements conducted on the surface of these islands show large, atomically flat, and defect-free terraces [Fig. 1(b)]. High-resolution STM topographies recorded on various islands show that their surface is terminated by a  $\text{Co}_3\text{Sn}$  layer, whose apparent height is dominated by the  $d$  orbitals of the Co atoms occupying the kagome lattice sites [Fig. 1(c)] [17]. This observation is consistent with the high substrate temperature  $T > 800$  °C during film deposition, which disfavors a stanene termination [25]. A detailed analysis of the  $\text{Co}_3\text{Sn}$  lattice structure [Fig. 1(a)] further reveals the presence of approximately 2% tensile strain along the [010] direction (crystallographic  $b$  axis), which presumably results from the lattice mismatch ( $\approx 5\%$ ) with the substrate.

The large density of states of electronic flat bands manifests as a sharp peak in the differential conductance ( $dI/dV$ )

spectrum of scanning tunneling spectroscopy (STS) measurements [23,26]. A typical  $dI/dV$  spectrum [Fig. 1(d)] recorded on the  $\text{Co}_3\text{Sn}$  surface is indeed dominated by a prominent double peak structure, which is located just below zero applied bias voltage  $V_B$ , i.e., just below Fermi energy  $E_F = eV_B$  ( $e$ , elementary charge). This observation is qualitatively consistent with previous studies [8,17] and *ab initio* calculations [Figs. 1(e) and 1(f), and the SM [5)] in which these LDOS peaks result from a set of kagome flat bands, which derive from the Co  $3d$  orbitals [22]. The first flat band (FB1) resides just below  $E_F$  and is mostly formed by  $d_{xy}$  and  $d_{x^2-y^2}$  orbitals. A second flat band (FB2) appears at lower energies and originates from the  $d_{xz}$  and  $d_{yz}$  orbitals. The pronounced  $dI/dV$  peak associated with the flat-band LDOS contrasts with our results from STM studies on thin films of the isostructural antiferromagnet FeSn (see the SM [5]). As with earlier studies of ferromagnetic  $\text{Fe}_3\text{Sn}_2$  [10], also  $dI/dV$  spectra recorded on the  $\text{Fe}_3\text{Sn}$  surface lack this distinct feature [12], because the electronic structures of FeSn and  $\text{Fe}_3\text{Sn}_2$  do not contain a kagome flat band, owing to strong magnetic exchange terms and disadvantageous layer stacking ( $\text{Fe}_3\text{Sn}_2$ ) [5,16].

The Wannier states of  $d$ -orbital-derived kagome flat bands are predicted to exhibit maximum charge density at the

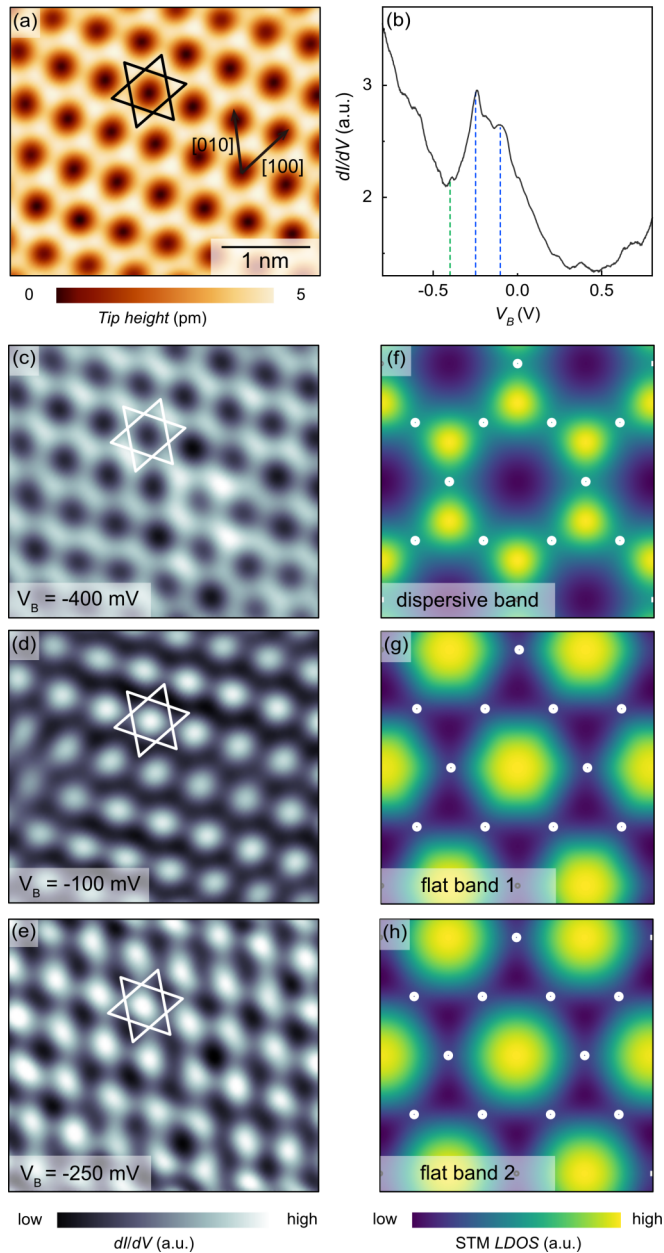


FIG. 2. (a) STM topography of the  $\text{Co}_3\text{Sn}$  surface ( $I = 3.5$  nA,  $V_B = 300$  mV). (b)  $dI/dV$  spectrum recorded within the field of view of panel (a). [(c)–(e)] Series of  $dI/dV$  maps recorded for various  $V_B$  values [see dashed lines panel (b)] in the same field of view as panel (a) ( $I = 3$  nA,  $V_m = 10$  mV) (see the SM [5]). The kagome lattice is schematically indicated. [(f)–(h)] The corresponding calculated local density of states (LDOS) of the dispersive band, as well as for flat bands 1 and 2, respectively (see the SM [5] for model details).

kagome lattice center [8]. We use spectroscopic imaging experiments with the STM to examine the real-space distribution of the associated LDOS. The spectroscopic map recorded at a bias voltage  $V_B = -400$  mV, which corresponds to an energy outside the flat-band  $dI/dV$  peak, is shown in Fig. 2(c). The spatial  $dI/dV$  distribution mirrors the corresponding STM topography [Fig. 2(a)], which is dominated by tunneling into the  $d$  orbitals of the  $\text{Co}_3\text{Sn}$  layer. Spectroscopic maps recorded within the flat-band  $dI/dV$  peak at  $V_B = -100$  mV and  $V_B =$

$-250$  mV exhibit a contrast reversal; an enhanced  $dI/dV$  amplitude is observed at the kagome lattice center, which is not occupied by a Co atom [Figs. 2(d) and 2(e)], and forms an effective triangular lattice. We note that the Sn atom at the kagome lattice center of the  $\text{Co}_3\text{Sn}$  layer [cf. Fig. 1(a)] contributes negligible spectral weight to the electronic structure at these energies and cannot account for the observed  $dI/dV$  characteristics (see the SM [5]). This observation is consistent with results from effective model calculations [22] in which the coupling between three Sn  $p$ -orbitals and three Co  $d$ -orbitals shifts their associated electronic bands to higher and lower energies.

To understand this phenomenology, we set up a minimal tight-binding model, which comprises of  $d_{x^2-y^2}$ ,  $d_{xy}$ ,  $d_{xz}$ , and  $d_{yz}$  orbitals per lattice site. STM simulations of the calculated real-space-resolved LDOS are shown in Figs. 2(f)–(h) (see the SM [5] for model details). The spectral weight associated with dispersive electron bands is found between the Co lattice sites and realizes an effective honeycomb pattern [Fig. 2(c)], consistent with our experimental observations [cf. Fig. 2(c)]. The STM simulations of the LDOS of flat bands 1 and 2 [Figs. 2(g) and 2(h)] also reproduce the contrast reversal seen in our spectroscopic mapping experiments [Figs. 2(d) and 2(e)], i.e., the spectral weight of the flat bands is localized at the kagome lattice center. We remark that the qualitative form of the computed LDOS can be understood by the combination of the shapes of the  $d$  orbitals and the texture of the kagome flat-band wave functions. As such, the qualitative feature of localized charge density inside the hexagons is expected to be robust even in case the flat band gains a finite dispersion through, e.g., spin-orbit coupling and out-of-plane hopping terms (see the SM [5]).

This observation of a contrast reversal serves as direct evidence for the nontrivial localization mechanism. It allows us to distinguish the flat-band electronic states from those of dispersive electron bands, as well as trivially localized states, such as well-localized orbitals and surface resonances, whose spectral weight would be localized at the Co atom positions. Interestingly, the distinction of the kagome flat-band Wannier state is challenging in case of  $s$ - and  $p$ -orbital derived flat bands, whose spectral weight would reside at the kagome lattice sites [9] (see the SM [5] for results on another CoSn island).

Previous theoretical studies of the Wannier states of the CoSn flat bands predict a localization length  $l \approx 7 \text{ \AA}$  [8]. Interestingly, our quantitative analysis of the spatial  $dI/dV$  distributions reveals much shorter values. Given the  $dI/dV$  peaks associated with the flat-band LDOS decay well within the honeycomb center, i.e., within the length scale of one unit cell, we can estimate  $l$  by applying Gaussian fits to representative  $dI/dV$  line cuts [see Figs. 3(a) to 3(d)]. The  $d_{xy}/d_{x^2-y^2}$ -derived FB1 exhibits localization lengths  $l_{\text{FB1}} = 2.6 \pm 0.1 \text{ \AA}$  and  $l_{\text{FB1}'} = 2.9 \pm 0.1 \text{ \AA}$  along the [100] and [010] directions, respectively. Similarly, the  $d_{xz}/d_{yz}$ -derived FB2 exhibits localization lengths  $l_{\text{FB2}} = 2.4 \pm 0.2 \text{ \AA}$  and  $l_{\text{FB2}'} = 3.4 \pm 0.5 \text{ \AA}$  along the [100] and [010] directions, respectively. While tensile strain along the [010] direction increases the localization length along this direction, the spectral weight remains predominantly localized at the kagome lattice center (nominal diameter  $\approx 7.4 \text{ \AA}$ ).



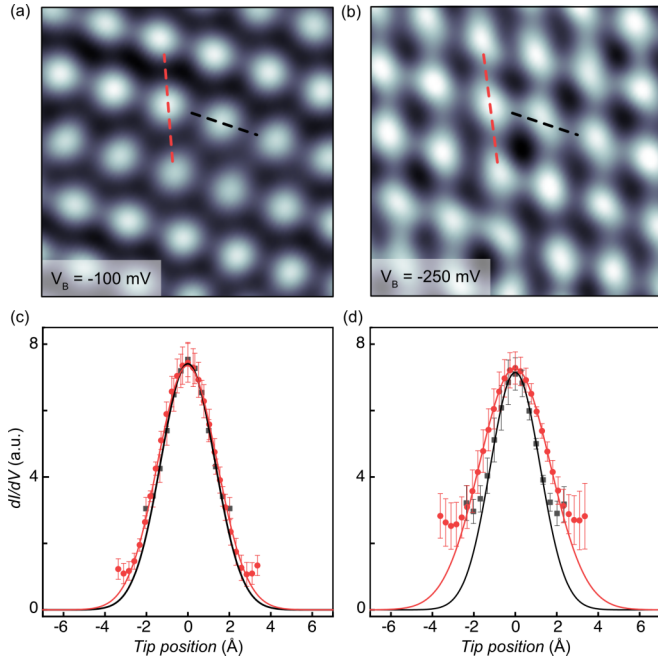


FIG. 3. [(a),(b)]  $dI/dV$  maps recorded at  $V_B = -100$  mV and  $V_B = -250$  mV, respectively ( $I = 3$  nA,  $V_m = 10$  mV). [(c),(d)]  $dI/dV$  amplitudes (solid symbols) extracted from the spectroscopic maps along the color-coded line profiles shown in panels (a) and (b), respectively. Gaussian fits to the data are shown as solid lines in the respective colors.

### III. DISCUSSION

The observed real-space localization suggests a moderate out-of-plane coupling between adjacent  $\text{Co}_3\text{Sn}$  layers, that is, the kagome flat bands of  $\text{CoSn}$  should exhibit a quasi-2D character. Unlike three-dimensional (3D) electronic states, which extend into the bulk, 2D electronic states can be strongly perturbed by surface defects, such as atoms [27] and step edges [28]. Here, we test the spatial dimension of the  $\text{CoSn}$  flat bands by recording  $dI/dV$  spectra along a line, which crosses two one-unit cell high step edges [Fig. 4(a)]. The  $dI/dV$  amplitude associated with the dispersive Co bands at  $V_B \leq -400$  mV weakly responds to the presence of the step edges [Fig. 4(b)]. This is consistent with the observed out-of-plane dispersion of these states [8] and indicates their 3D character. By contrast, the  $dI/dV$  amplitude at  $-350$  mV  $\leq V_B \leq -70$  mV is strongly suppressed at the step edges and decays over a distance of less than one nanometer toward the edge [Fig. 4(c)]. This observation indicates the quasi-2D nature of the kagome flat bands of  $\text{CoSn}$ , consistent with their observed vanishing out-of-plane dispersion [8,17].

The suppression of the flat-band LDOS near atomic step edges permits the presence of a localized edge state in the same energy range [Fig. 4(b)]. Spatial mapping of the  $dI/dV$  amplitude confirms the one-dimensional edge state character of this spectral feature [Fig. 4(d)]. Its nonuniform real space distribution along the edge indicates its dependence on the edge termination. We analyze the characteristic decay length  $\zeta$  of this edge state into the quasi-2D bulk to estimate the quasi-particle velocity  $v$  of the kagome flat bands. We extract  $\zeta \approx 5$  Å by fitting its spatial decay with a Gaussian [Fig. 4(d) inset]

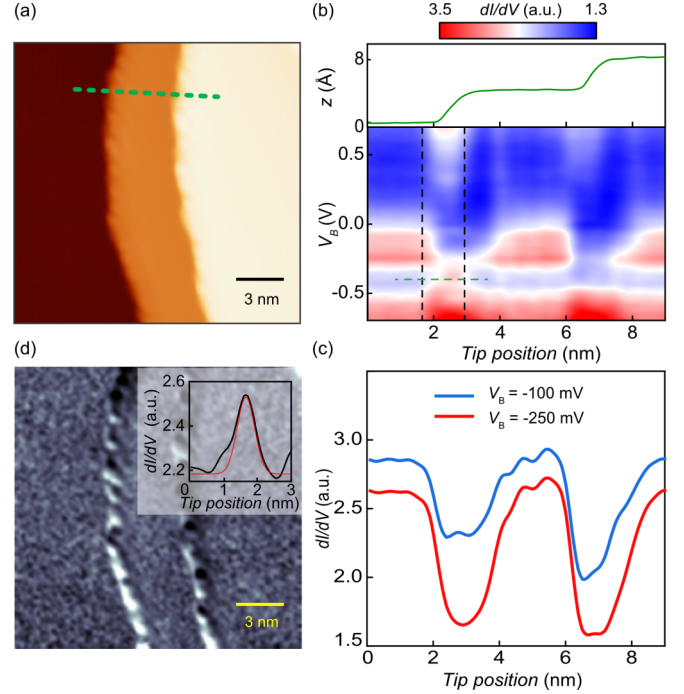


FIG. 4. (a) STM topography of the  $\text{Co}_3\text{Sn}$  surface, which exhibits two one unit cell step edges ( $I = 2.5$  nA,  $V_B = 400$  mV). (b) (Upper panel) The topographic height  $z$  profile along the green line in panel (a). (Bottom panel)  $dI/dV$  spectra recorded along along the green line in panel (a) plotted as a function of tip position and  $V_B$  ( $I = 2$  nA,  $V_m = 10$  mV). The edge region is indicated by the vertical pair of dashed lines. We note that the spatial modulation of the flat-band  $dI/dV$  is only faintly visible, because it is obscured by the set-point effect present in these line-cut measurements. (c)  $dI/dV$  amplitude at  $V_B = -100$  mV and  $V_B = -250$  mV plotted as a function of the tip position along the green line in panel (a) ( $I = 2$  nA,  $V_m = 10$  mV). (d)  $dI/dV$  amplitude recorded in the field of view of panel (a) at  $V_B = -350$  mV. The inset displays the position-dependent  $dI/dV$  amplitude along the horizontal green dashed line in panel (b).

and estimate  $v = (\zeta \Delta_{\text{SOC}})/h$  ( $h$  denotes Planck's constant). Previous measurements of the electronic structure of  $\text{CoSn}$  detected a spin-orbit coupling (SOC) induced spectral gap  $\Delta_{\text{SOC}} \approx 80$  meV at the  $\Gamma$  point between  $-300$  and  $-400$  meV [8]. Using these parameters, we obtain  $v \approx 1 \times 10^4$  m/s. This value is quantitatively comparable to the theoretical estimate  $v^* \approx 5 \times 10^3$  m/s in a simple tight-binding approximation  $E \approx t \cos(ka)$  ( $k$ , crystal momentum) for a calculated hopping parameter  $t \approx 15$  meV between the flat-band Wannier states [8].

Finally, we comment on the topological character of the  $\text{CoSn}$  flat band [8]. Interestingly, a SOC-induced spectral gap at the  $\Gamma$  point imbues the kagome flat band in the 2D limit with a nontrivial  $\mathbb{Z}_2 = 1$  index. Our tight-binding model calculations (see the SM [5]) of one  $\text{CoSn}$  layer (1 unit-cell thickness, 40-unit cells width) indeed show the presence of 1D edge states (see the SM [5]). They appear at the flat-band energy and connect the flat bands with the dispersive bulk bands over a large energy range. However, these states appear both in case SOC is included and excluded. SOC merely induces a spectral

splitting. The opening of a nontrivial  $\Delta_{\text{SOC,DFT}} \approx 50$  meV due to SOC [8] could reconnect the edge states with the bulk bands to accommodate the  $\mathbb{Z}_2 = 1$  index. However, we cannot resolve these details in our calculations, owing to the presence of metallic bulk states. Further STM experiments with magnetic scattering centers [29] could help to clarify the origin of these edge states.

#### IV. CONCLUSION

Our experimental study demonstrates the real-space localization of electrons occupying a native kagome flat band. Spectroscopic mapping measurements with the STM allowed us to directly visualize the LDOS of the corresponding flat-band electronic states, which result from destructive electron interference. This nontrivial localization mechanism results in a unique real-space distribution of the LDOS of  $d$ -orbital-derived flat bands by which they can be distinguished from the LDOS of dispersive bands and trivially localized states, such as well-localized orbitals and surface resonances. While interlayer and spin-orbit coupling, and a more complex lattice structure appearing under realistic conditions are generally believed to counteract the localization mechanism of destructive interference, described by the 2D kagome lattice model, our results show that the electronic states of a kagome flat band can remain localized despite these effects.

Our quantitative analyses further show that the Wannier states of the CoSn flat bands are localized with  $l \approx 2 - 3$  Å, a value much smaller than theoretically expected [8]. This strong localization is concomitant with a significantly renormalized  $v \approx 1 \times 10^4$  m/s. Our findings contrast with moiré

superlattice materials where the larger spatial extent (e.g.,  $\approx 15$  nm for magic-angle twisted bilayer graphene) of the flat-band Wannier functions [30] affords a comparably small Coulomb on-site repulsion  $U \approx 20$  meV [2,26]. Hence, the enhancement of interaction effects in the flat bands of CoSn due to a large  $U \approx 5 - 6$  eV [8] could be even more pronounced than previously thought [31].

Together, our observations establish transition-metal based kagome metals as a promising venue to explore the emergence of interacting many-body states in a topological flat band at potentially elevated temperatures [6,7,13]. We anticipate that chemical [32] and modulation doping [33], as well as lattice strain [8] (see the SM [5] for a discussion of tensile strain observed in our study) offer rich opportunities to realize partial flat-band occupations at which these effects are expected to appear.

#### ACKNOWLEDGMENTS

This work has been primarily supported by the Hong Kong RGC (Grant. No. 26304221) and the Croucher Foundation (Grant. No. CIA22SC02) awarded to B.J. K.T.L. acknowledges the support of the Ministry of Science and Technology, China, and the Hong Kong RGC (Grants. No. 2020YFA0309600, No. RFS2021-6S03, No. C6025-19G, No. AoE/P-701/20, No. 16310520, No. 16310219, and No. 16307622). H.C.P. acknowledges support of the Hong Kong RGC (Grant. No. 26308021) and the Croucher Foundation (Grant. No. CF21SC01). C.C. acknowledges support from the Tin Ka Ping Foundation.

- 
- [1] Y. Cao, V. Fatemi, S. Fang, K. Watanabe, T. Taniguchi, E. Kaxiras, and P. Jarillo-Herrero, Unconventional superconductivity in magic-angle graphene superlattices, *Nature (London)* **556**, 43 (2018).
- [2] Y. Cao, V. Fatemi, A. Demir, S. Fang, S. L. Tomarken, J. Y. Luo, J. D. Sanchez-Yamagishi, K. Watanabe, T. Taniguchi, E. Kaxiras *et al.*, Correlated insulator behaviour at half-filling in magic-angle graphene superlattices, *Nature (London)* **556**, 80 (2018).
- [3] Y. Tang, L. Li, T. Li, Y. Xu, S. Liu, K. Barmak, K. Watanabe, T. Taniguchi, A. H. MacDonald, J. Shan *et al.*, Simulation of Hubbard model physics in WSe<sub>2</sub>/WS<sub>2</sub> moiré superlattices, *Nature (London)* **579**, 353 (2020).
- [4] E. C. Regan, D. Wang, C. Jin, M. I. Bakti Utama, B. Gao, X. Wei, S. Zhao, W. Zhao, Z. Zhang, K. Yumigeta *et al.*, Mott and generalized Wigner crystal states in WSe<sub>2</sub>/WS<sub>2</sub> moiré superlattices, *Nature (London)* **579**, 359 (2020).
- [5] See Supplemental Material at <http://link.aps.org/supplemental/10.1103/PhysRevResearch.5.043269> for information on the materials characterization, additional experimental data, and details of the model calculations.
- [6] K. Sun, Z. Gu, H. Katsura, and S. Das Sarma, Nearly flat-bands with nontrivial topology, *Phys. Rev. Lett.* **106**, 236803 (2011).
- [7] H.-M. Guo and M. Franz, Topological insulator on the kagome lattice, *Phys. Rev. B* **80**, 113102 (2009).
- [8] M. Kang, S. Fang, L. Ye, H. C. Po, J. Denlinger, C. Jozwiak, A. Bostwick, E. Rotenberg, E. Kaxiras, J. G. Checkelsky *et al.*, Topological flat bands in frustrated kagome lattice CoSn, *Nat. Commun.* **11**, 4004 (2020).
- [9] Z. Li, J. Zhuang, L. Wang, H. Feng, Q. Gao, X. Xu, W. Hao, X. Wang, C. Zhang, K. Wu *et al.*, Realization of flat band with possible nontrivial topology in electronic kagome lattice, *Sci. Adv.* **4**, eaau4511 (2018).
- [10] Z. Lin, J.-H. Choi, Q. Zhang, W. Qin, S. Yi, P. Wang, L. Li, Y. Wang, H. Zhang, Z. Sun, L. Wei, S. Zhang, T. Guo, Q. Lu, J. H. Cho, C. Zeng, and Z. Zhang, Flatbands and emergent ferromagnetic ordering in Fe<sub>3</sub>Sn<sub>2</sub> kagome lattices, *Phys. Rev. Lett.* **121**, 096401 (2018).
- [11] J.-X. Yin, S. S. Zhang, G. Chang, Q. Wang, S. S. Tsirkin, Z. Guguchia, B. Lian, H. Zhou, K. Jiang, I. Belopolski *et al.*, Negative flat band magnetism in a spin-orbit-coupled correlated kagome magnet, *Nat. Phys.* **15**, 443 (2019).
- [12] D. Multer, J.-X. Yin, M. S. Hossain, X. Yang, B. C. Sales, H. Miao, W. R. Meier, Y.-X. Jiang, Y. Xie, P. Dai *et al.*, Imaging real-space flat band localization in kagome magnet FeSn, *Commun. Mater.* **4**, 17 (2023).
- [13] E. Tang, J.-W. Mei, and X.-G. Wen, High-temperature fractional quantum Hall states, *Phys. Rev. Lett.* **106**, 236802 (2011).
- [14] T. Neupert, L. Santos, C. Chamon, and C. Mudry, Fractional quantum Hall states at zero magnetic field, *Phys. Rev. Lett.* **106**, 236804 (2011).

- [15] L. Ye, M. Kang, J. Liu, F. Von Cube, C. R. Wicker, T. Suzuki, C. Jozwiak, A. Bostwick, E. Rotenberg, D. C. Bell *et al.*, Massive Dirac fermions in a ferromagnetic kagome metal, *Nature (London)* **555**, 638 (2018).
- [16] M. Kang, L. Ye, S. Fang, J.-S. You, A. Levitan, M. Han, J. I. Facio, C. Jozwiak, A. Bostwick, E. Rotenberg *et al.*, Dirac fermions and flat bands in the ideal kagome metal FeSn, *Nat. Mater.* **19**, 163 (2020).
- [17] Z. Liu, M. Li, Q. Wang, G. Wang, C. Wen, K. Jiang, X. Lu, S. Yan, Y. Huang, D. Shen *et al.*, Orbital-selective Dirac fermions and extremely flat bands in frustrated kagome-lattice metal CoSn, *Nat. Commun.* **11**, 4002 (2020).
- [18] J.-X. Yin, N. Shumiya, S. Mardanya, Q. Wang, S. S. Zhang, H.-J. Tien, D. Multer, Y. Jiang, G. Cheng, N. Yao *et al.*, Fermion-boson many-body interplay in a frustrated kagome paramagnet, *Nat. Commun.* **11**, 4003 (2020).
- [19] S. Sankar, R. Liu, X.-J. Gao, Q.-F. Li, C. Chen, C.-P. Zhang, J. Zheng, Y.-H. Lin, K. Qian, R.-P. Yu *et al.*, Experimental evidence for Berry curvature multipoles in antiferromagnets, [arXiv:2303.03274](https://arxiv.org/abs/2303.03274).
- [20] B. C. Sales, W. R. Meier, D. S. Parker, L. Yin, J. Q. Yan, A. F. May, S. Calder, A. A. Aczel, Q. Zhang, H. Li *et al.*, Flat-band itinerant antiferromagnetism in the kagome metal  $\text{CoSn}_{1-x}\text{In}_x$ , [arXiv:2201.12421](https://arxiv.org/abs/2201.12421).
- [21] W. R. Meier, M.-H. Du, S. Okamoto, N. Mohanta, A. F. May, M. A. McGuire, C. A. Bridges, G. D. Samolyuk, and B. C. Sales, Flat bands in the CoSn-type compounds, *Phys. Rev. B* **102**, 075148 (2020).
- [22] Y. Jiang, H. Hu, D. Călugăru, C. Felser, S. Blanco-Canosa, H. Weng, Y. Xu, and B. A. Bernevig, Kagome Materials II: SG 191: FeGe as a LEGO Building Block for the Entire 1:6:6 series: hidden d-orbital decoupling of flat band sectors, effective models and interaction Hamiltonians, [arXiv:2311.09290](https://arxiv.org/abs/2311.09290).
- [23] G. L. Li, A. Luican, J. M. B. Lopes dos Santos, A. H. Castro Neto, A. Reina, J. Kong, and E. Y. Andrei, Observation of van Hove singularities in twisted graphene layers, *Nat. Phys.* **6**, 109 (2010).
- [24] H. Li, S. Li, M. H. Naik, J. Xie, X. Li, J. Wang, E. Regan, D. Wang, W. Zhao, S. Zhao *et al.*, Imaging moiré flat bands in three-dimensional reconstructed  $\text{WSe}_2/\text{WS}_2$  superlattices, *Nat. Mater.* **20**, 945 (2021).
- [25] F.-F. Zhu, W.-J. Chen, Y. Xu, C.-L. Gao, D.-D. Guan, C.-H. Liu, D. Qian, S.-C. Zhang, and J.-F. Jia, Epitaxial growth of two-dimensional stanene, *Nat. Mater.* **14**, 1020 (2015).
- [26] Y. Xie, B. Lian, B. Jäck, X. Liu, C.-L. Chiu, K. Watanabe, T. Taniguchi, B. A. Bernevig, and A. Yazdani, Spectroscopic signatures of many-body correlations in magic-angle twisted bilayer graphene, *Nature (London)* **572**, 101 (2019).
- [27] E. J. Heller, M. F. Crommie, C. P. Lutz, and D. M. Eigler, Scattering and absorption of surface electron waves in quantum corrals, *Nature (London)* **369**, 464 (1994).
- [28] I. K. Drozdov, A. Alexandradinata, S. Jeon, S. Nadj-Perge, H. Ji, R. J. Cava, B. Andrei Bernevig, and A. Yazdani, One-dimensional topological edge states of bismuth bilayers, *Nat. Phys.* **10**, 664 (2014).
- [29] B. Jäck, Y. Xie, B. Andrei Bernevig, and A. Yazdani, Observation of backscattering induced by magnetism in a topological edge state, *Proc. Natl. Acad. Sci. USA* **117**, 16214 (2020).
- [30] H. C. Po, L. Zou, A. Vishwanath, and T. Senthil, Origin of Mott insulating behavior and superconductivity in twisted bilayer graphene, *Phys. Rev. X* **8**, 031089 (2018).
- [31] H. Huang, L. Zheng, Z. Lin, X. Guo, S. Wang, S. Zhang, C. Zhang, Z. Sun, Z. Wang, H. Weng *et al.*, Flat-band-induced anomalous anisotropic charge transport and orbital magnetism in kagome metal CoSn, *Phys. Rev. Lett.* **128**, 096601 (2022).
- [32] B. C. Sales, W. R. Meier, A. F. May, J. Xing, J.-Q. Yan, S. Gao, Y. H. Liu, M. B. Stone, A. D. Christianson, Q. Zhang, M. A. McGuire *et al.*, Tuning the flat bands of the kagome metal CoSn with Fe, In, or Ni doping, *Phys. Rev. Mat.* **5**, 044202 (2021).
- [33] S. Cheng, B. Wang, I. Lyalin, N. Bagués, A. J. Bishop, D. W. McComb, and R. K. Kawakami, Atomic layer epitaxy of kagome magnet  $\text{Fe}_3\text{Sn}_2$  and Sn-modulated heterostructures, *APL Mat.* **10**, 061112 (2022).